Physica B: Physics of Condensed Matter xxx (2017) 1–4

Contents lists available at ScienceDirect

Physica B: Physics of Condensed Matter

journal homepage: www.elsevier.com/locate/physb

Weak-ferromagnetism of CoF_3 and FeF_3

Sanghyun Lee [a,*], Shuki Torii [a,b], Yoshihisa Ishikawa [a,b], Masao Yonemura [a,b,c], Taketo Moyoshi [d], Takashi Kamiyama [a,b,c,**]

[a] Institute of Materials Structure Science, KEK, Tokai 319-1106, Japan
[b] J-PARC Center, KEK, Tokai 319-1106, Japan
[c] Sokendai(The Graduate University for Advanced Studies), Tokai 319-1106, Japan
[d] Neutron Science and Technology Center, CROSS, Tokai 319-1106, Japan

ARTICLE INFO

Keywords:
Weak-ferromagnetism
Dzyaloshinski-Moriya interaction
Time-of-flight neutron powder diffractometer

ABSTRACT

Cobalt trifluoride CoF_3 and Iron trifluoride FeF_3 are known as a G-type antiferromagnetic structure in the *R*-3*c* rhombohedral crystal structure. The neutron powder diffraction study had been reported that Co antiferromagnetic spin direction is parallel to 3-fold crystal axis in CoF_3 whereas Fe antiferromagnetic spin direction is perpendicular to 3-fold crystal axis in FeF_3. However, the resolution of early neutron powder diffractometer is not enough to distinguish between $(003)_h$ and $(101)_h$ rhombohedral magnetic peaks definitely.

We employed high-resolution powder neutron diffractometer(SuperHRPD) at room temperature in MLF, J-PARC. The time-of-flight neutron powder diffractometer distinguishes clearly between $(003)_h$ and $(101)_h$ magnetic peaks. Then, we confirmed the proposed magnetic structural models of CoF_3 and FeF_3 at room temperature. In a magnetic susceptibility, CoF_3 displays the additional magnetic anomaly at $T^* = 40$ K. We discussed possible weak-ferromagnetism by the interplay of spin tilting and Dzyaloshinski-Moriya interactions.

1. Introduction

For last several decades, the instrumental resolution of neutron powder diffractometers has been improved a lot than early neutron diffractometer. As compared with the angle dispersive diffractometer, the highest resolution can be achieved by time-of-flight neutron powder diffractometer with increasing neutron flight distance and focusing on high angle position of detector. Super High Resolution Powder Diffractometer (SuperHRPD) is time-of-flight neutron powder diffractometer installed at Materials and Life Science Experimental Facility(MLF), in J-PARC [1,2]. Up to date, it achieved the highest resolution neutron powder diffractometer with $\Delta d/d = 0.035\%$ by optimized conditions among cutting-edge neutron powder diffractometers.

Such a high-resolution neutron powder diffractometer is utilized to investigate detailed crystal and magnetic structure simultaneously. In another word, it can characterize the symmetry of order-parameter precisely which is essential concepts in the Landau theory of phase transition. Landau free energy is expanded in the polynomials of order-parameters by symmetrical constraint [3]. If any tiny distortion gives different symmetry of order-parameters, it cannot be neglected simply. Recently, we reported that symmetrically different spin directions are important to understanding the phase transition mechanism and magnetoelastic couplings in MnO, CoO, and NiO [4].

Cobalt trifluoride CoF_3 and iron trifluoride FeF_3 are other good examples why detailed spin directions are important to understanding weak-ferromagnetism [5]. Both have a G-type antiferromagnetic structure in *R*-3*c* rhombohedral crystal structure [6,7]. E. O. Wollan et al. reported magnetic structure that Co spin is parallel while Fe spin is perpendicular to 3-fold crystal axis [7]. If G-type antiferromagnetic spin directions are perpendicular to 3-fold crystal axis as like FeF_3, Dzyaloshinski-Moriya(DM) interaction induces weak-ferromagnetism in a hexagonal plane [5,8–10]. However, the poor resolution of early neutron diffractometer could not distinguish the rhombohedral peaks clearly [7]. Thus, it is necessary to reinvestigate the magnetic structure with distinguished rhombohedral peaks.

2. Material and methods

We used commercial powder sample of CoF_3 and FeF_3 from Sigma Aldrich. To minimize reaction with water from the atmosphere, we treated powder sample under inert gas in the glove box. We checked the sample quality in X-ray diffraction using single wavelength $K_{\alpha 1}$ of Cu

* Corresponding author.
** Corresponding author. Institute of Materials Structure Science, KEK, Tokai 319-1106, Japan.
E-mail addresses: lee@post.j-parc.jp (S. Lee), takashi.kamiyama@kek.jp (T. Kamiyama).

https://doi.org/10.1016/j.physb.2017.11.082
Received 8 August 2017; Received in revised form 21 November 2017; Accepted 27 November 2017
Available online xxxx

target by Rigaku Smartlab. Magnetic susceptibility was measured by SQUID magnetometer (MPMS, Quantum Design) in the user laboratory of CROSS. The time-of-flight powder neutron diffraction was done at room temperature by SuperHRPD beamline in MLF, J-PARC. We filled powder sample 1.5 g approximately in Φ6 mm V-Ni cylindrical sample can. We used high-resolution 90-degree bank data instead of super-high-resolution backscattering data for Rietveld analysis. In contrast to back-scattering bank, 90-degree bank can cover the longer d-spacing while differentiating both $(003)_h$ and $(101)_h$ magnetic peaks. Therefore, d-range and resolution of 90-degree bank are optimized for this study. We employed Z-Rietveld [11,12] and Fullprof program [13] to do Rietveld analysis for X-ray and neutron diffraction data respectively.

3. Results

In Fig. 1 of XRD pattern, CoF_3 sample shows no impurity phase with high background due to Co fluoresce affected by Cu target. On the other hand, we found the impurity phase of $FeF_3{\cdot}3H_2O$ for FeF_3 as-purchased sample [14,15]. The mass ratio of impurity $FeF_3{\cdot}3H_2O$ is about 10%.

Figs. 2 and 3 display the magnetic susceptibility and magnetization curves for both CoF_3 and FeF_3. The antiferromagnetic transition of CoF_3 is reported at $T_N = 460$ K [7] which is out of our measurement range, only up to 400 K. We found the additional magnetic anomaly at $T^* = 40$ K. Even though we could not find the impurity peaks in XRD, we discuss the possible contribution of cobalt difluoride CoF_2 which has antiferromagnetic transition occasionally close to $T^* = 40$ K. CoF_2 magnetic susceptibility is decreasing while cooling down to lowest temperature [16]. Its temperature dependence behavior is quite different from Fig. 2a. Weak ferromagnetism appears with small magnetic hysteresis at 5 K in the inset of Fig. 3a. Since CoF_2 antiferromagnetic spin is parallel to

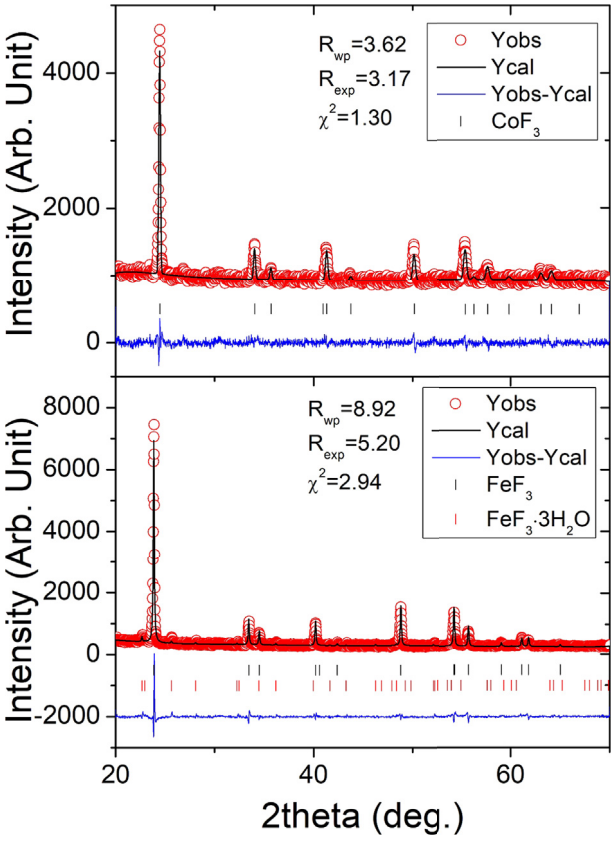

Fig. 1. Room-temperature XRD for (a) CoF_3 and (b) FeF_3. Due to Cu X-ray target, CoF_3 shows the fluorescence effect of high backgrounds. We measured as-purchased CoF_3 and FeF_3. But, $FeF_3{\cdot}3H_2O$ impurity phase coexists with FeF_3.

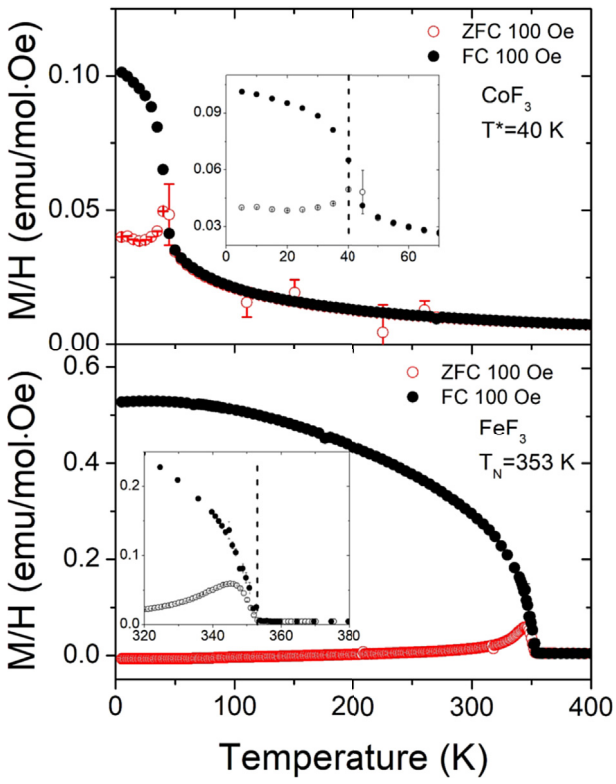

Fig. 2. Temperature dependence of magnetic susceptibility for (a) CoF_3 and (b) FeF_3. The antiferromagnetic transition of CoF_3 is reported at $T_N = 460$ K [7]. While further cooling, the possible spin canting transition of CoF_3 is observed at $T^* = 40$ K. FeF_3 shows magnetic transition at $T_N = 353$ K with coexistence between G-type antiferromagnetic moment $A_{x,y}$ and weak-ferromagnetic moment $F_{x,y}$.

4-fold crystal axis without weak-ferromagnetism [17], T^* is considered as another magnetic phase transition of CoF_3 below T_N.

On the other hand, the antiferromagnetic transition of FeF_3 is observed at $T_N = 353$ K less than reported 364.8(5) K by Mössbauer spectroscopy [18], 367 K [19] by antiferromagnetic resonance, and 394 K by neutron powder diffraction [7]. High purity sample is necessary to judge if impurity can reduce antiferromagnetic transition temperature. The antiferromagnetic transition of β-$FeF_3{\cdot}3H_2O$ is 14.7 K which is far away from T_N of FeF_3 [15]. Therefore, observed magnetic hysteresis is the signature of weak-ferromagnetism in FeF_3. Weak-ferromagnetism of FeF_3 is consistent with previous references [20].

In Fig. 4, by employing time-of-flight neutron powder diffractometer at room temperature, we clearly distinguished between $(003)_h$ and $(101)_h$ magnetic peaks experimentally in *R*-3*c* (Glazer tilting $a^-a^-a^-$) rhombohedral structure distorted from ideal cubic perovskite *Pm*-3*m* (Glazer tilting $a^0a^0a^0$). Previously, E. O. Wollan et al. analyzed magnetic models by the intensity ratios between $(003)_h$ and $(101)_h$ magnetic peaks [7]. But, early neutron powder diffractometer could not separate these rhombohedral peaks clearly. In Fig. 4, $(003)_h$ magnetic peak of CoF_3 is zero while ones of FeF_3 is non-zero intensity.

In the *R*-3*c* rhombohedral structure with magnetic propagation vector k=(0 0 0), the representational analysis gives magnetic models $\Gamma_{mag} = \Gamma_1(A_g) + \Gamma_3(A_{2g}) + 2\Gamma_5(E_g)$ in Ref. [10] and Table 1. CoF_3 and FeF_3 have G-type antiferromagnetic spin spatial distribution through 180-degree superexchange interactions in the geometry of corner sharing octahedral. Co antiferromagnetic spin direction is parallel to 3-fold crystal axis in CoF_3 whereas Fe antiferromagnetic spin direction is perpendicular to 3-fold crystal axis in FeF_3. The magnetic structure of CoF_3 and FeF_3 are $\Gamma_1(A_g)$ and $\Gamma_5(E_g)$ magnetic model respectively. Finally, we confirm the proposed magnetic models again by high-resolution neutron powder diffraction. Rietveld analysis result are given in Table 2.

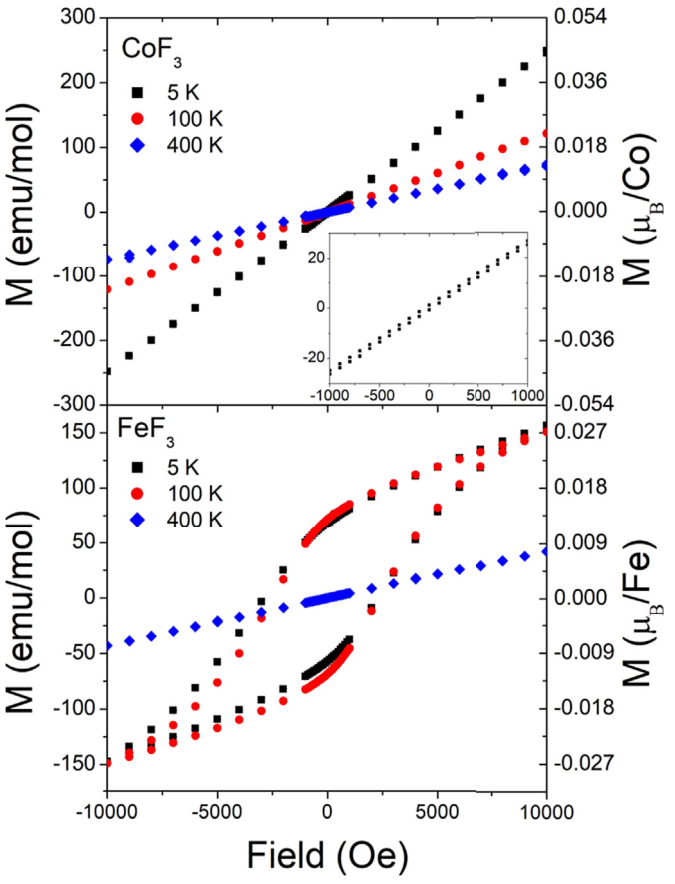

Fig. 3. Field dependence of magnetization at 5, 100, and 400 K for (a) CoF_3 and (b) FeF_3. (a inset) Small magnetic hysteresis of CoF_3 are observed at 5 K.

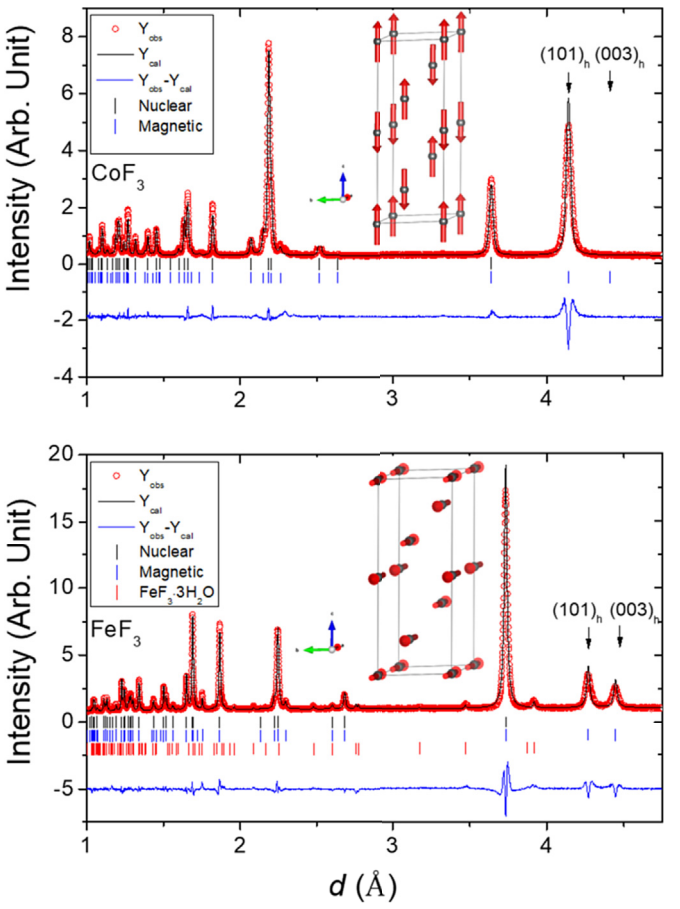

Fig. 4. Rietveld analysis of magnetic models for (a) CoF_3 and (b) FeF_3 in *R*-3*c*. Longer d-range of 90-degree bank data is analyzed, instead of backscattering bank, to cover $(003)_h$ and $(101)_h$ magnetic peaks. CoF_3 spin directions are parallel with 3-fold crystal symmetry whereas FeF_3 spin directions are perpendicular to 3-fold symmetry in *R*-3*c*.

4. Discussion

Magnetic representational analysis characterizes order-parameter symmetry in Ref. [10] and Table 1. Antiferromagnetic order parameter A_j and weak-ferromagnetic order parameter F_j are given by

$$A_j = M_{1,j} - M_{2,j};\ F_j = M_{1,j} + M_{2,j};\ i = TM1, TM2;\ j = x, y, z$$

The i symbol stands for TM1 (0, 0, 0) and TM2 (0, 0, 0.5) transition-metal positions. Subscript of *x*, *y* represent specific spin directions in a hexagonal *a*-*b* plane and *z* represents along c-axis respectively. Since both $A_{x,y}$ and $F_{x,y}$ belong to same irreducible representation, $A_{x,y}$ antiferromagnetic order induces $F_{x,y}$ weak-ferromagnetic order through the bilinear coupling in Landau free energy. If we have the physical constraints such as same TM1 and TM2 magnetic moments $|M_{1,j}| = |M_{2,j}|$, antiferromagnetic A_j and weak-ferromagnetic F_j order parameter direction should be perpendicular to each other relatively. If A_j and F_j directions are parallel with each other, TM1 and TM2 magnetic moment size can be different $|M_{1,j}| \neq |M_{2,j}|$. On the one hand, with respect to the crystallographic axis, precise antiferromagnetic spin directions $A_{x,y}$ are unknown in the hexagonal *a*-*b* plane [18]. Therefore, weak-ferromagnetic spin directions are also unknown in the hexagonal *a*-*b* plane too. We know only that weak-ferromagnetic spin direction $F_{x,y}$ is perpendicular to antiferromagnetic spin directions $A_{x,y}$ in the hexagonal *a*-*b* plane.

T. Moriya introduced antisymmetric exchange interactions, so-called Dzyaloshinski-Moriya interaction [9], which is given by $H_{DM} = \mathbf{D}_{ij}\cdot[\mathbf{S}_i \times \mathbf{S}_j]$. When antiphase octahedral rotation occurs from *Pm*-3*m*($a^0a^0a^0$) to *R*-3*c*($a^-a^-a^-$), the crystal point symmetry of fluorine atoms, which mediated between neighbor transition-metals, reduced from 4/*mm.m* (centrosymmetric) to .2 (non-centrosymmetric) point symmetry. By Moriya's rule, net DM vector $\mathbf{D}_{ij}$ is parallel to 3-fold crystal axis and positioned on fluorine non-centrosymmetric points.

In the superposition of same irreducible representation for both antiferromagnetic moment $A_{x,y}(\Gamma_5)$ and weak ferromagnetic moment $F_{x,y}(\Gamma_5')$, spin cross vector $\mathbf{S}_i \times \mathbf{S}_j$ is parallel with DM vector $\mathbf{D}_{ij}$. Then, DM interaction reduces the energy if $A_{x,y}(\Gamma_5)$ antiferromagnetic moment is canted inside hexagonal plane. When antiferromagnetic moment $A_z(\Gamma_1)$ combined with weak ferromagnetic moment $F_{x,y}(\Gamma_5')$, spin cross vector $\mathbf{S}_i \times \mathbf{S}_j$ is perpendicular to DM vector $\mathbf{D}_{ij}$. In this case, DM interaction does not reduce the energy.

In contrast to FeF_3, CoF_3 antiferromagnetic spin $A_z(\Gamma_1)$ is parallel to 3-fold crystal axis. Then, DM interactions couldn't induce the weak-ferromagnetism in CoF_3. However, we observed the weak-ferromagnetism of CoF_3 below 40 K. As we discuss that $A_{x,y}$ antiferromagnetic spin inside hexagonal plane can induces $F_{x,y}$ weak-

Table 1
Magnetic structural model by representational analysis from Yu. A. Izyumov and V.E. Naishi [10]. In *R*-3*c* with magnetic propagation vector *k*=(0 0 0), $\Gamma_5(E_g)$ antiferromagnetic model and $\Gamma_5'(E_g)$ weak-ferromagnetic model belongs to same irreducible representations.

R-3*c* with *k*=(0 0 0)	TM1 (0 0 0)	TM2 (0 0 0.5)	Order-parameter
$\Gamma_1(A_g)$	(0 0 S_z)	(0 0 -S_z)	$A_z = M_{1z} - M_{2z}$
$\Gamma_3(A_{2g})$	(0 0 S_z)	(0 0 S_z)	$F_z = M_{1z} + M_{2z}$
$\Gamma_5(E_g)$	(S_x S_y 0)	(-S_x -S_y 0)	$A_{x,y} = M_{1x,y} - M_{2x,y}$
$\Gamma_5'(E_g)$	(S_x S_y 0)	(S_x S_y 0)	$F_{x,y} = M_{1x,y} + M_{2x,y}$

Table 2
Rietveld results of CoF_3 and FeF_3 in *R*-3*c* rhombohedral structure. Co/Fe atom position is Wyckoff 6b (0 0 0) and F atom position is 18e (x, 0. 25). The point symmetry of Co/Fe and F are −3 and .2 respectively. Fe antiferromagnetic spin direction is arbitrary inside *R*-3*c* hexagonal plane.

R-3*c*, *k*=(0 0 0)	CoF_3 $\Gamma_1(A_g)$ model	FeF_3 $\Gamma_5(E_g)$ model
$a = b$ (Å)	5.03473(8)	5.2030(1)
c (Å)	13.2228(5)	13.3361(5)
F x	0.6048(1)	0.5854(2)
Co/Fe B_{iso} (Å^2)	0.12(6)	0.19(5)
F B_{iso} (Å^2)	0.85(2)	0.93(6)
Magnetic moment (μ_B)	3.21(1)	2.60(2)
R_p (%)	6.13	5.12
R_{wp} (%)	8.23	7.06
R_{exp} (%)	3.87	2.29
χ^2 (%)	4.52	9.53
R_{mag} (%)	6.92	8.46

ferromagnetism by magnetic representational analysis and microscopic DM interactions, Co antiferromagnetic spin A_z will be rotated from 3-fold crystal symmetry that additional $A_{x,y}$ component can induces weak-ferromagnetism of CoF_3 below T^*.

5. Conclusions

By distinguishing $(003)_h$ and $(101)_h$ rhombohedral peaks clearly, we confirmed the reported magnetic structure for both CoF_3 and FeF_3 at room temperature. We observed additional magnetic anomaly of CoF_3 below $T^* = 40$ K by SQUID magnetometer. There is the possible antiferromagnetic spin rotation that induces the weak-ferromagnetism of CoF_3 at 40 K.

Acknowledgement

We appreciate Kaoru Namba, Masahiro Shioya, Katsumi Shimizu, Kazutaka Ikeda for their technical assistance of neutron powder diffraction. In addition, we thank Masato Hagihala for fruitful discussion and Ayu Nur Ika Puji for checking English grammar. Magnetic susceptibility measurements were performed by using the SQUID magnetometer (MPMS, Quantum Design Inc.) at the CROSS user laboratory. The neutron diffraction experiments using SuperHRPD were carried out under the S-type project with Proposal No. 2014S05. This work was supported by JSPS KAKENHI Grant Number JP16K17758.

References

[1] S. Torii, M. Yonemura, T. Yulius Surya Panca Putra, J. Zhang, P. Miao, T. Muroya, R. Tomiyasu, T. Morishima, S. Sato, H. Sagehashi, et al., J. Phys. Soc. Jpn. 80 (Suppl. B) (2011) SB020.
[2] S. Torii, M. Yonemura, Y. Ishikawa, P. Miao, R. Tomiyasu, S. Satoh, Y. Noda, T. Kamiyama, J. Phys. Conf. Ser. 502 (2014) 012052.
[3] J. Toledano, P. Toledano, The Landau Theory of Phase Transitions: Application to Structural, Incommensurate, Magnetic and Liquid Crystal Systems, vol. 3, World Scientific Publishing Co Inc, 1987.
[4] S. Lee, Y. Ishikawa, P. Miao, S. Torii, T. Ishigaki, T. Kamiyama, Phys. Rev. B 93 (6) (2016) 064429.
[5] Y.A. Izyumove, V.E. Naish, R.P. Ozerov, Neutron Diffraction of Magnetic Materials, Consultants Bureau, 1991.
[6] M.A. Hepworth, K.H. Jack, R.D. Peacock, G.J. Westland, Acta Cryst. 10 (1957) 63.
[7] E. Wollan, H. Child, W. Koehler, M. Wilkinson, Phys. Rev. 112 (4) (1958) 1132.
[8] I. Dzialoshinski, J. Phys. Chem. Solids 4 (1958) 241.
[9] T. Moriya, Phys. Rev. 120 (1960) 91.
[10] Yu A. Izyumov, V.E. Naishi, J. Magn. Magn. Mater. 12 (1979) 239.
[11] R. Oishi, M. Yonemura, Y. Nishimaki, S. Torii, A. Hoshikawa, T. Ishigaki, T. Morishima, K. Mori, T. Kamiyama, Nucl. Instr. Meth. Phys. Rev. A 600 (2009) 94.
[12] R. Oishi-Tomiyasu, M. Yoneumra, T. Morishima, A. Hoshikawa, S. Torii, T. Ishigaki, T. Kamiyama, J. Appl. Cryst. 45 (2012) 229.
[13] J. Rodriguez-Carvajal, Phys. B Condens. Matter 192 (1993) 55.
[14] G. Teufer, Acta Crystallogr. 17 (1964) 1480.
[15] I. Dezsi, et al., J. Phys. C8 (1988) 1463.
[16] D.N. Astrov, A.S. Borovik-Romanov, M.P. Orlova, J. Exptl. Theor. Phys. 33 (1957) 812.
[17] A.N. Bazhan, Ch Bazan, Zh. Eksp. Teor. Fiz. 69 (1975) 1768.
[18] G.K. Wertheim, H.J. Guggenheim, D.N.E. Buchanan, Solid Sate Commnun. 5 (1967) 537.
[19] P. Hagenmuller, et al., Inorganic Solid Fluorides: Chemistry and Physics, Elsevier, 2012.
[20] J.R. Shane, M. Kestigian, J. Appl. Phys. 39 (1968) 1027.